Journal of Structural Geology, Vol. 9, No. 4, pp. 393 to 401, 1987
Printed in Great Britain

0191-8141/87 $03.00 + 0.00

Normal fault geometry related to sediment compaction and burial

IAN DAVISON

Curso de Pós-Graduação em Geologia, Instituto de Geociências—Universidade Federal da Bahia, 40.210—Salvador, Bahia, Brazil

(*Received* 1 *May* 1986; *accepted in revised form* 24 *November* 1986)

Abstract—Field observations are presented on meso-scale normal faults and sandstone dikes which cross-cut turbidites in the petroliferous Recôncavo Basin situated in Bahia, NE Brazil. Two discrete phases of normal faulting occurred. It is argued that the first was probably active during the first 200 m of burial. Compaction estimates from folded sandstone dikes and the accommodation patterns of shale bedding planes around ball-and-pillow structures were made. First-phase fault profiles were initially reasonably straight but refraction on the fault planes increased due to the differing compaction between sandstone and shale. The later phase of faulting occurred at a greater depth, with steeper fault dips and strong refraction of fault planes at lithological boundaries. This greater fault refraction is probably the result of burial and diagenesis, which increased the difference in rheological properties between sandstone and shale before faulting occurred. Thus, complex superposed fault geometries may be developed by changing rheological properties and stress conditions during progressive burial. It is shown that sandstone dikes were not always intruded vertically. Injected dikes cannot be used in the same manner that Neptunian dikes are conventionally used to estimate tectonic strain, if independent evidence of the original orientation of the dike is not available.

INTRODUCTION

PRICE (1966) summarized the theoretical aspects of normal fault geometry; he showed that rheology, pore pressure, stress regime and original heterogeneities are important factors controlling fault profiles. Later workers, such as Proffett (1977), Crans *et al.* (1980), Wernicke & Burchfiel (1982) and Gibbs (1983, 1984), have provided detailed theoretical and descriptive accounts which show that displacement history, amount of extension and, occasionally, compaction are also important controlling factors on normal fault geometry. This paper concentrates on the effects of sediment compaction and burial on fault profiles, and describes profiles where estimates of sediment compaction were possible.

The field examples described are from the Island of Itaparica which is situated in the Cretaceous Recôncavo Basin in NE Brazil (Fig. 1). Lower Cretaceous turbidites, with very regular parallel bedding, consisting of sandstone, siltstone and shale, outcrop continuously along the coast of Itaparica Island. These provide excellent sub-horizontal multilayers for fault studies. The sedimentological aspects of this sequence have been described by Zalan *et al.* (1981).

EARLY NORMAL FAULTS

Field mapping indicates that there is a reasonably close spatial relationship between early normal faults and upwardly injected sandstone dikes (Fig. 1). In several localities sandstone dikes intrude upwards and feed into fault planes. In Fig. 2(a) the sandstone dike only enters the fault plane when it reaches the sandstone bed and there is no offset of the dike across the fault, which suggests that it was intruded after faulting. Other dikes are offset by low-angle faults. Thus, early faulting and dike injection are thought to be broadly contemporaneous. The dikes may be due to seismically induced de-watering, which is supported by the spatial correlation between faulting and dike intrusion. However, this would be difficult to prove conclusively.

A typical example of an early normal fault is shown in Fig. 2(b). There is no consistent rotation between the beds on either side of the fault, although localized drag is present in the adjacent shales. Refraction on the fault plane, to a steeper angle (38°) occurs through two sandy siltstone layers, and the angle drops to 12° in the shales. When fault planes cut sandstone and sandy siltstones they usually appear as discrete planes which are 1–2 mm thick, but the faults usually broaden out into a narrow ductile sheared zone up to 1–2 cm thick within the shales. This is an indication that the shales were only weakly compacted, as a single fracture plane would be difficult to produce in highly porous shales. Faults always die out in shales. Most of these early faults have throws of less than 0.5 m and profile lengths of less than 5 m. No mineralization or brecciation was observed associated with these faults. The strike of the faults is generally N25°E which is parallel to the regional fault trend in the Recôncavo Basin (Ghignone 1972).

A histogram of fault dip indicates that the faults measured adjacent to shales show a range of dips between 7 and 45°, but the majority are clustered between 7 and 24° (Fig. 4). The occasional higher dips may be explained by varying lithologies of the shales. The sandstone measurements have significantly higher fault dips, varying between 30 and 45°. The maximum fault refraction between sandstone and shale reaches 25° for any one fault. This fault dip/lithology histogram could be useful in any faulted terrain to analyse statistically which lithologies produce ramps and flats.

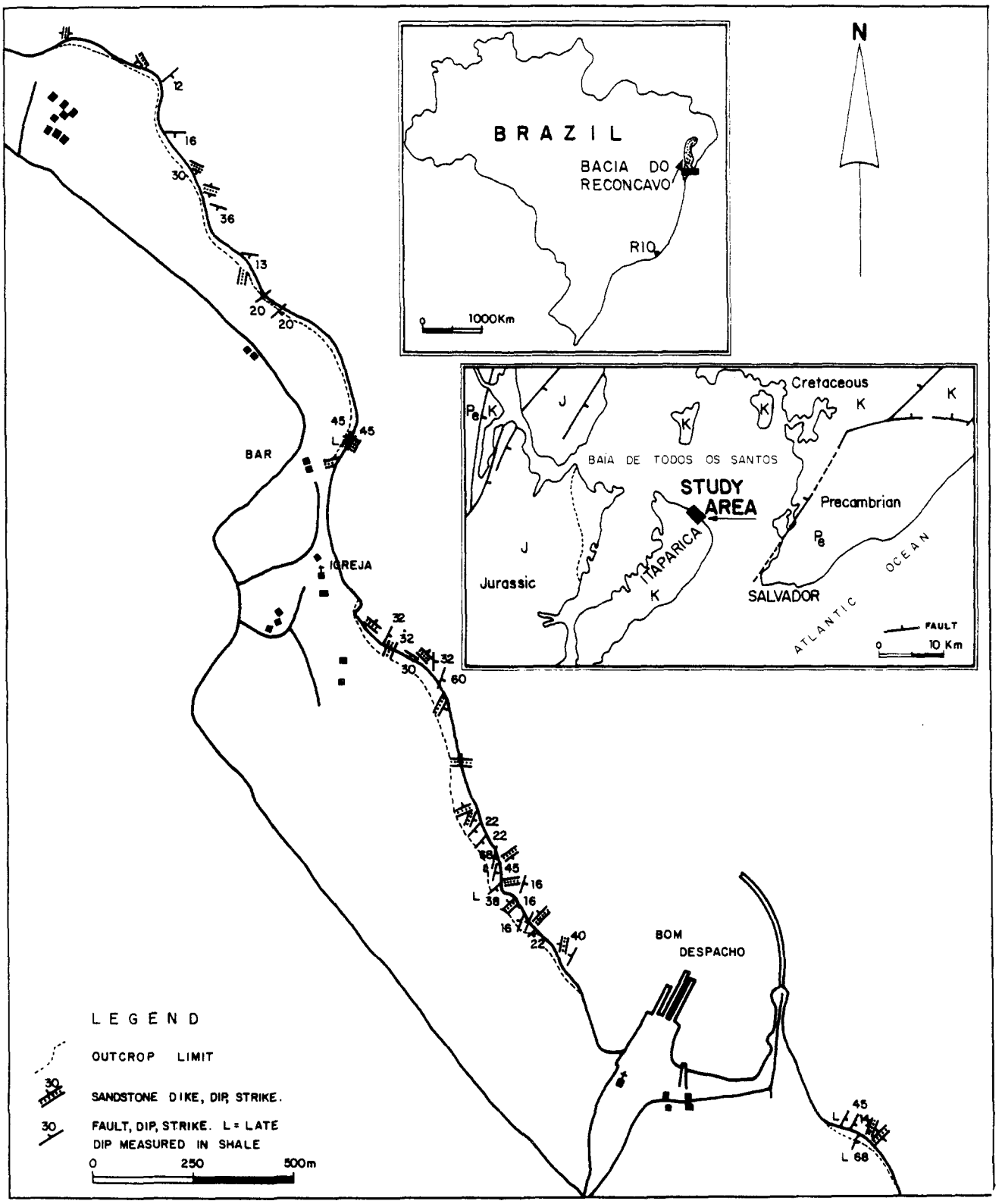

Fig. 1. Map showing the distribution of faults and sandstone dikes. Note the close spatial relationship between early faults and dikes. Fault dips and dike dips are measured in shales because the fault dip varies between sandstones and shales (see text). Inset maps show location of the study area.

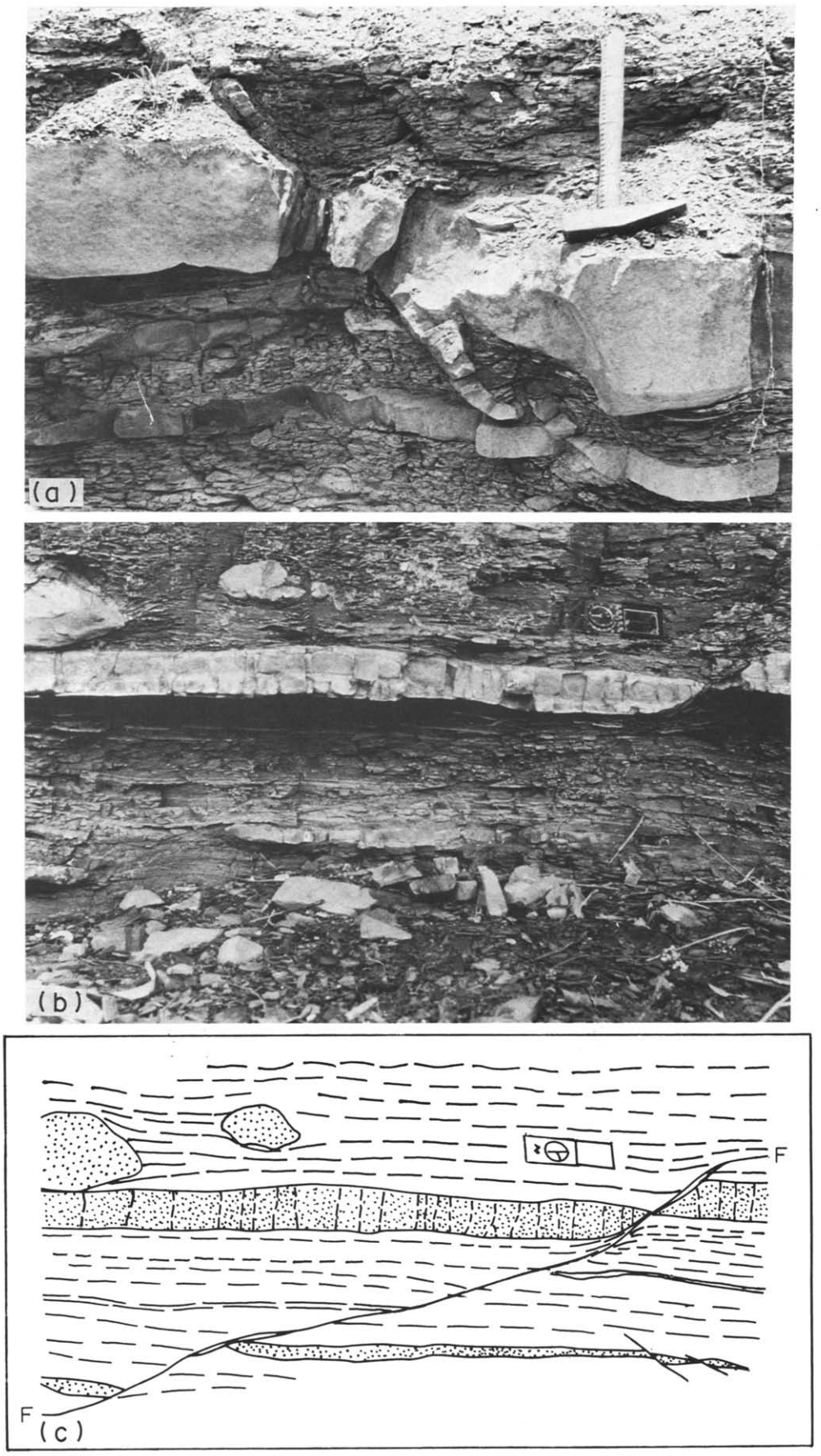

Fig. 2.(a) Sandstone dike injected up into a fault plane. The hammer is 30 cm long. (b) Low-angle early normal fault refracted through siltstone layers. Ball-and-pillow structures with shale bedding plane deflection used to calculate relative compaction, are also shown. The compass is 16 cm long. (c) Line drawing of early normal fault, shown in (b).

Fig. 3.(a) Later, steeper normal fault with a horse developed due to a later fault cutting-out the rugosity caused by refraction of the earlier fault plane through thick sandstone. Fault 1 was the first fault followed by faults 2 and 3. The lens cap is 5 cm diameter. (b) Sandstone dikes which have subsequently been folded and faulted by compaction. The compass is 10 cm long.

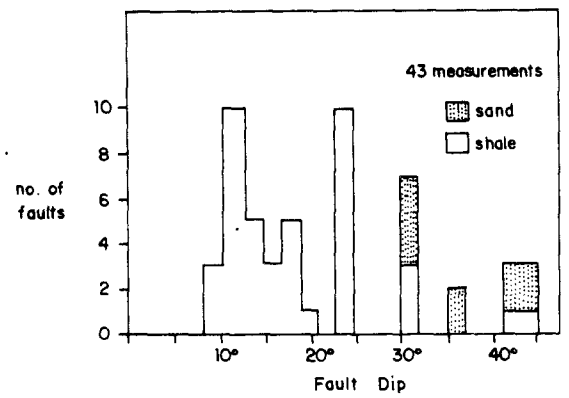

Fig. 4. Histogram of fault dip annotated for lithology (sandstone or shale) adjacent to the dip measurement.

LATER NORMAL FAULTS

A later set of faults, which have associated breccias and are mineralized with calcite and haematite, cross-cut the earlier low-angle faults. The later faults have steeper angles (35–90°) and displacements are usually greater than 0.3 m. Anastomosing structures are often observed on these faults, with fault horses surrounded by fault planes (Fig. 3a). The initial fault plane was probably number 1 and the ultimate fault plane number 3 (Fig. 3a). Some fault horses are rotated so that bedding is parallel to the fault plane (Fig. 5). These horses can be attributed to an original fault refraction between sandstone and shale, followed by later straighter faults which bypass the refraction to produce a smoother profile.

Fault plane refraction reaches 45° in extreme cases. This is probably due to the large differences in rheology and applied deviatoric stress across each bed, between the already-cemented sandstone and possibly overpressured shale.

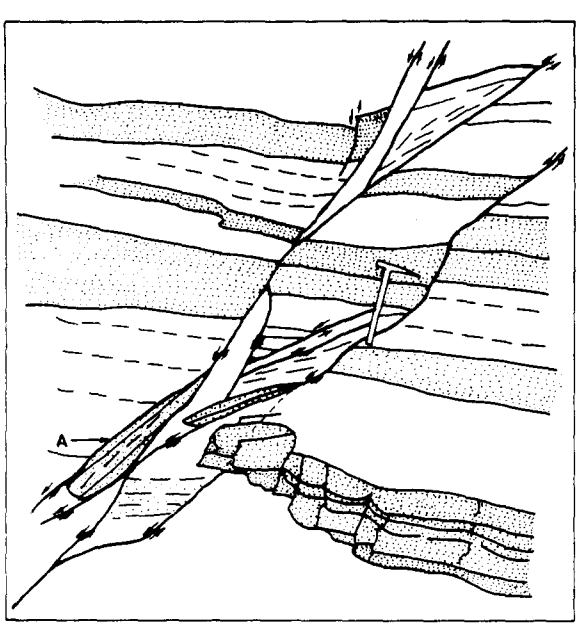

Fig. 5. Complex sequence of later steeply dipping faults. In block A the bedding is parallel to the fault plane. Note the large refractions of the fault planes between lithological contacts. Stippled beds are sandstone, the rest is shale. The hammer is 30 cm long.

COMPACTION ESTIMATES

The effect of compaction by porosity reduction is often defined as a homogeneous volume loss, where original angular relationships would be unaffected. Observation of the injected sandstone dikes in the study area strongly suggests that compaction can be approximated as a vertical shortening with no horizontal shortening. The effect of compaction has been to fold and, in some cases, fault the dikes when they cut through shales (Fig. 3b). Faults were classified as 'compaction faults' where both lower and upper tips were contained within an individual shale bed, suggesting that tip strains were taken up by compaction. The axial planes of the folded dikes are always sub-horizontal and parallel to bedding, whatever the final orientation of the folded dike train.

The fold axes of the dikes are straight to slightly curved and sub-horizontal, suggesting there was only one direction of shortening, which was vertical. If there had been homogeneous volume loss, the fold axes should be strongly curved as there would be a simultaneous horizontal and vertical shortening. These observations also indicate that the sandstone dikes approximate to initially tabular bodies. Shelton (1962) came to a similar conclusion on the tabular shape of dikes.

During compaction the sandstone dikes buckled and probably rotated and thickened. The two latter components were not quantified. It was possible to calculate the buckling component of shortening along the final direction of the folded dike train using the 'piece of string' method, where the dikes were assumed to be initially tabular (Fig. 6). A total of 18 dikes were measured, with shortening varying from 10 to 60%. The maximum values were recorded by the thinnest vertical dikes. Shortening appears to depend on factors such as original dike thickness, dike and shale lithology, folding mechanism and initial dike orientation. There is also the possibility of variation in the timing of injection. The

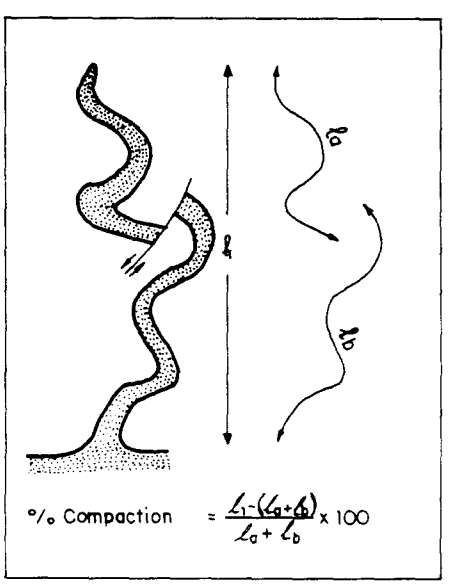

Fig. 6. Method used to calculate the shortening produced by compaction after dike injection. Both buckling and accommodation microfaults have been considered.

number of variables makes it very difficult to ascertain the relative importance of each independently.

The maximum buckle shortening of 60% is taken as a reasonable estimate of shale compaction after dike injection. It is recognized that some layer-parallel shortening and porosity loss may have occurred prior to buckling, which would increase the compaction estimate. Density measurements on the shales indicate they still retain a surface porosity of 20–25% (surface density is 2.25 g cm^{-3}). The total compaction of the shales, at their maximum burial depth, may have reduced the porosities by a further 7% to 13–18%. Hamilton (1976) estimates porosity rebound effects of this order when sediments are uplifted to the surface from depths of 1 km or more. Hamilton (1971, 1976) quotes surface porosities as high as 86% in deep-water claystones. Therefore the shales could not have lost much porosity before dike injection, considering their minimum burial porosity was around 13–18% and 60% compaction was effected after dike intrusion. A 60% compaction of the shales places a limit on the depth where dike injection and synchronous normal faulting took place. Argillaceous sediments should be compacted to 60% porosity or less in the first 200 m of burial in normally compacted sediments (Fig. 7). If overpressuring had occurred 60% porosity may have been preserved down to greater depths. However, near surface overpressuring is rare in sedimentary basins (Magara 1976). Thus early normal faulting is thought to have occurred at relatively shallow burial depths.

The observation that the shales were compacted to approximately 13–18% porosity at maximum burial, implies burial depths of 1.0–1.3 km (using density/porosity curves of Hamilton 1976). The subsequent exhumation of this turbidite sequence remains to be explained in the context of the regional tectonics, but this problem will not be discussed further here.

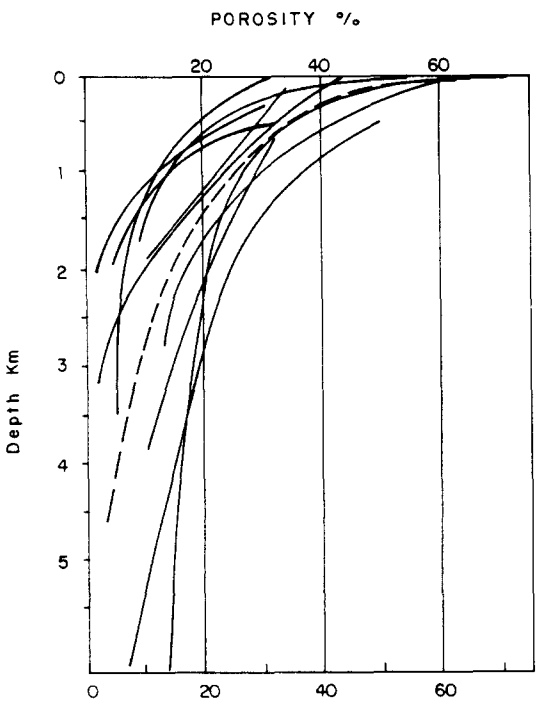

Fig. 7. Porosity decrease with depth of burial in argillaceous sediments. The dotted line is an average decrease which was used in calculating the compaction effects in Fig. 11. (Taken from Reike & Chilingarian 1974.)

Most of the dikes have final orientations which lie well away from the vertical. The lowest dip recorded was 30° and many lie between 40 and 70°. The amount of vertical pure shear, without horizontal strain, required to rotate a near-vertical (>85°) dike to a dip of 40° or less would be greater than −95%, which is an excessive compaction if this alone was responsible for rotation of near-vertical dikes to lower dips. Bedding-parallel simple shear cannot explain the low dips either, as dikes dip to both north and south within the same shale bed. It is argued therefore that the dikes were not intruded perpendicular to the horizontal bedding. Borradaile (1984) concluded that most Neptunian dikes (where material is infilled from above) are oriented at right angles to bedding and has successfully used these structures to make tectonic strain measurements (Borradaile 1979). However, in the light of the observations above, upwardly injected dikes could not be used if independent evidence of the original orientation of the dike was not available.

The sandstones and siltstones often form ball-and-pillow structures within the shales, due to loading near to the sediment surface (Fig. 2b). By observing shale bedding planes accommodated around the sandstone bodies, it was possible to calculate the relative vertical compaction between sandstone and shales (Fig. 8). Baldwin (1971) assigned the name 'decompaction number' to the average ratio shown in Fig. 8. The term, relative compaction of shale to sandstone, is preferred here, because Baldwin simplified the rationale of this type of calculation by assuming that the sandstone did not compact at all. His 'decompaction number' was assumed to give the total compaction of the shale.

Sandstones do compact, although the quantity is difficult to estimate if original porosity is not known. In fully-compacted, normally-pressured clean sandstones, porosities of 20–30% are common at depths of 3 km or more. Further reduction in porosity is probably produced by chemical processes involving dissolution and precipitation rather than mechanical reorganization of grains. If precipitation mechanisms such as intergranular carbonate deposition occur, this leads to reduction in porosity but not necessarily compaction. Hamilton (1976) quoted the average surface porosity ranges for

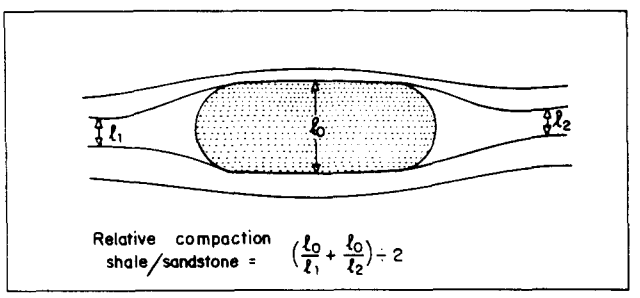

Fig. 8. Calculation used to measure the relative compaction between sandstone balls and shales.

deep-water silty sand to coarse sand, as 52–38%, respectively. Assuming a similar range of initial porosities for the sandstones examined here, and considering that the present porosity of the thickest sandstones is about 25–30% (calculated using thin sections and density measurements), this gives a rough guide to the compaction expected in the sandstones: 8–27%.

Measurement of 10 sandstone balls gave a relative vertical compaction of shale to sandstone ranging from 2 to 4 (average 2.6). This means that starting with equal thicknesses of uncompacted shale and sandstone, the compacted shale now ranges from one-half to one-quarter of the thickness of the compacted sandstone. These measurements place further constraints on the total compaction of the shales since deposition. This can be illustrated by considering a reasonable total sandstone compaction of 15% and the average relative compaction of shale to sandstone of 2.6, which gives a total shale compaction of $100 - (100 - 15)/2.6 = 67\%$. This value broadly corroborates the earlier statement that the minimum shale compaction after faulting was 60%, as some compaction had probably occurred before faulting. In summary, the shales are thought to have compacted between about 60 and 70% since early faulting, and the sandstones between 15 and 25% since deposition, but perhaps as little as 10–15% since faulting.

DECOMPACTION OF FAULT PROFILES

The dip of the early faults passing through shales generally ranges from 12 to 24° (Fig. 4). These fault planes can be decompacted if we consider them as passive planar markers which were subjected to a homogeneous vertical compaction without horizontal strain. It is questionable whether fault planes act as passive rotating planar markers during compaction; further displacement could have occurred during compaction as well as fluid expulsion along the fault. But considering that the fault displacements are small, these 'active' effects on final geometry are probably minor. Using a shale decompaction figure of 60%, the decompacted fault dips steepen-up and range from 28 to 47°. The present-day fault dips passing through the sandstones vary between 30 and 44°. Probably the most realistic decompaction factor for the sandstones since faulting is around 15%, which gives initial fault dips of 35–49°, which are close to the decompacted dip values for the shales. This result suggests that the initial fault dips in sandstones and shales were roughly equal and varied between about 35 and 50°, and that the subsequent compaction was responsible for shallowing of the fault dip and the refraction of the fault planes through angles of up to 25° between different lithologies.

These relatively low initial fault angles may be explained by a small surface slope and overpressuring in the sediments (Bartley & Glazner 1985). However, as noted above near surface overpressuring is rare in sedimentary basins. No direct evidence of palaeo-overpressuring has been observed but this would be difficult to see anyway. Bishop (1979) described overpressured zones as "now you see them now you don't". If this mechanism was not responsible, the low initial fault angles remain unexplained.

DISCUSSION

Analysis of field observations indicates that early normal faults were formed at relatively shallow burial depths in uncompacted sediments. However, it is not known if these small faults relate to larger growth faults associated with delta progradation in the Recôncavo Basin (Klein *et al.* 1972). Large-scale soft sediment slumping structures occur at only one locality in the study area and faults from this slump were not included in the analysis.

The initial faulting angles of early normal faults in both the sandstone and shales are thought to be in the range 30–49°. On subsequent compaction the fault dips passing through shales shallow to 12–24°. Faults passing through sandstones, which compact much less than the shales, are flattened only slightly to dips of 30–45°. This difference in compaction enhances refraction of fault planes up to 25° at lithological boundaries. The later and steeper normal faults have steeper angles partly due to the fact that the sediments were already compacted, thus preventing the passive rotation which affected earlier faults, but also due to the changing rheologies of the sediments. These faults show a very large refraction angle at lithological boundaries, suggesting there was a larger difference between the rheological properties and applied differential stresses between sandstone and shales than during the earlier phase of faulting. It would be impossible to produce the 45° refraction angles observed by differential compaction alone. Thus variable fault profiles and dips can be produced by these changing parameters during burial (Fig. 9). This may explain the faulting complexity in some regions where low-angle faults are cut by higher-angle faults, without recourse to early faults being rotated to lower angles by later ones (e.g. Proffett 1977).

Differential compaction causes large fault refraction angles when faulting occurs near to the surface and subsequent burial to 1 km or more ensues; growth faults are therefore particularly prone to compactional effects. If faulting occurs when rocks are already buried to depths of 1 km or more then fault refraction and flattening, caused by compaction, are minimal.

Another interesting effect of passive pure vertical compaction of fault planes is that the throw and displacement will decrease but heave will remain the same (Fig. 10).

Burial of a pre-existing fault plane can result in a variety of fault shapes depending on the degree of compaction, original fault shapes and timing of compaction in relation to faulting (Magara 1978). An example of just a few fault shapes which can be produced is shown in Fig. 11. Curve A is a listric fault developed from a growth fault in shale which is continually propagating

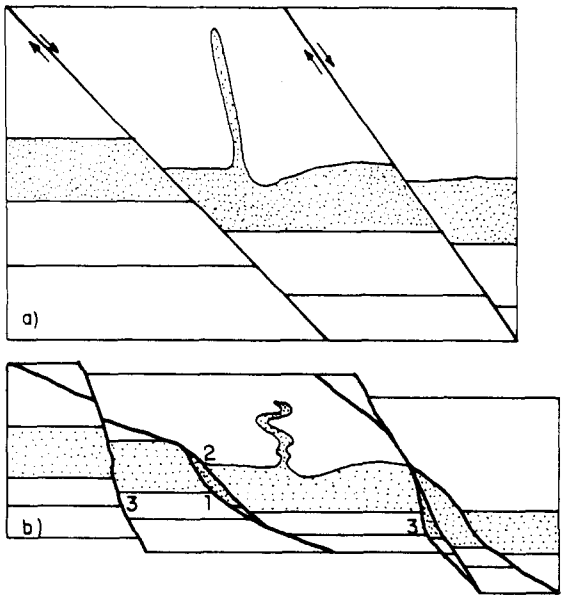

Fig. 9.(a) Cartoon explanation of faulting and compaction sequence. Normal fault (50° dip) and sandstone dikes injected within 200 m of the surface. (b) After 60% shale compaction the normal faults are at a lower angle and fault refraction is produced by differential sand/shale compaction (1); a new fault forms which straightens the active fault profile (2); the sandstone dike becomes folded and a new fault with a steeper angle, large refraction and anastamosing pattern cross-cuts the earlier low angle faults (3). The resulting complex fault pattern is due not only to passive fault rotation during compaction but also to the variation of stress conditions and rheological properties produced by burial and continued faulting at different depths.

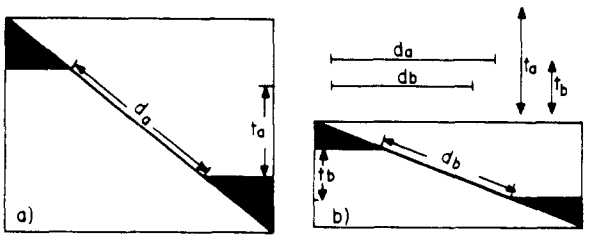

Fig. 10.(a) Simple normal fault with net displacement, d_a, and vertical throw, t_a. (b) Same fault after 50% compaction with vertical compaction but no horizontal strain: fault displacement is now, d_b, with a throw t_b; heave remains constant.

near the surface with an angle of 50°. The degree of compaction was calculated from an average porosity reduction with depth in shales (Fig. 7). The listric shape is solely due to compaction. This shape can be destroyed by further burial without faulting at the surface (curves B and C, Fig. 11). If the original fault is planar and extends to the surface, an upward flattening fault can be produced by further burial (Curve D in Fig. 11). It is interesting to note that on a seismic time section the curvatures in A and B would be further enhanced, but the convex fault in D would be straightened.

Acknowledgements—Comments of two anonymous referees considerably improved and tightened-up this work. The author would like to thank the Secretaria das Minas e Energia do Estado da Bahia for financial help. Natanael Gomes was responsible for the artwork.

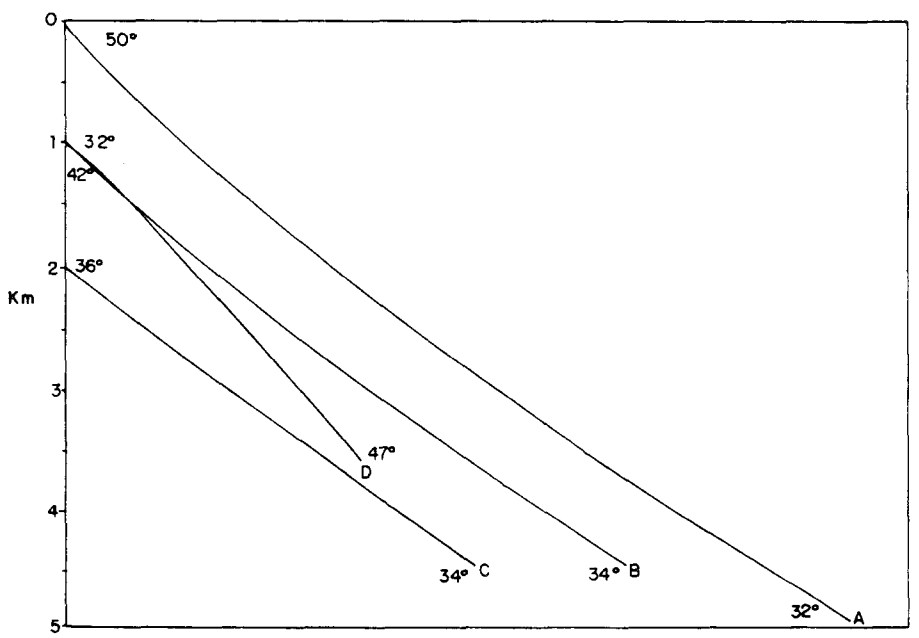

Fig. 11. Theoretical compaction effects on fault shapes. Horizontal = vertical scale. Curve A: listric fault produced by continuous burial of a continuously propagating planar fault with a 50° fault dip at the surface. The compaction is modelled using vertical compaction with no horizontal strain and porosity values from the dotted curve in Fig. 7. Curve B: represents further burial of curve A by 1 km. The dip at the top of the fault is 42°. Curve C: flattening of curve A after 2 km of additional burial. Curve D: fault produced after additional burial of 1 km of a planar fault with a 50° dip throughout its original length from 0 to 2.5 km. Dip at the top of the fault is flattened to 32°.

REFERENCES

Baldwin, B. 1971. Ways of deciphering compacted sediments. *J. sedim. Petrol.* **41**, 293–301.

Bartley, J. M. & Glazner, A. F. 1985. Hydrothermal systems and Tertiary low angle normal faulting in the southwestern United States. *Geology* **13**, 562–564.

Bishop, R. S. 1979. Calculated compaction states of thick abnormally pressured shales. *Bull. Am. Ass. Petrol. Geol.* **63**, 918–933.

Borradaile, G. J. 1979. Strain study of the Caledonides in the Islay region, SW Scotland: implications for strain histories and deformation mechanisms in greenschists. *J. geol. Soc. Lond.* **136**, 77–88.

Borradaile, G. J. 1984. A note on sand dike orientation. *J. Struct. Geol.* **6**, 587–588.

Crans, W., Mandl, G. & Haremboure, J. 1980. On the theory of growth faulting: a geomechanical delta model based on gravity sliding. *J. Petrol. Geol.* **2**, 265–307.

Ghignone, J. I. 1972. A evolução estrutural do Recôncavo durante o tempo Candeias. *Rev. Bras. Geociênc.* **2**, 35–50.

Gibbs, A. D. 1983. Balanced cross-section construction from seismic sections in areas of extensional tectonics. *J. Struct. Geol.* **5**, 153–160.

Gibbs, A. D. 1984. Structural evolution of extensional basin margins. *J. geol. Soc. Lond.* **141**, 609–620.

Hamilton, E. L. 1971. Elastic properties of marine sediments. *J. geophys. Res.* **76**, 579–604.

Hamilton, E. L. 1976. Variations of density and porosity with depth in deep sea sediments. *J. sedim. Petrol.* **46**, 280–300.

Klein, de Vries, G., Melo, U. & Favera, D. C. J. 1972. Subaqueous gravity processes on the front of Cretaceous deltas, Recôncavo Basin. *Bull. geol. Soc. Am.* **83**, 1469–1492.

Magara, K. 1976. Thickness of removed sedimentary rocks, palaeopore pressure and palaeotemperature, south western part of Western Basin. *Bull. Am. Ass. Petrol. Geol.* **60**, 554–565.

Magara, K. 1978. *Compaction and Fluid Migration.* Developments in Petroleum Science 9. Elsevier, Amsterdam.

Price, N. J. 1966. *Fault and Joint Development in Brittle and Semi-brittle Rock.* Pergamon Press.

Proffett, J. M. 1977. Cenozoic geology of the Yerington district, Nevada, and implications for the nature and origin of Basin and Range faulting. *Bull. geol. Soc. Am.* **88**, 247–266.

Reike, H. H., III & Chilingarian, G. V. 1974. *Compaction of Argillaceous Sediments.* Developments in Sedimentology 16. Elsevier, Amsterdam.

Shelton, J. W. 1962. Shale compaction in a section of Cretaceous Dakota Sandstone, northwestern, North Dakota. *J. sedim. Petrol.* **32**, 873–877.

Wernicke, B. & Burchfiel, B. C. 1982. Modes of extensional tectonics. *J. Struct. Geol.* **4**, 105–115.

Zalan, P. V., Rivas, A. J. P., Herter, G. G., Froes, J. C. R., Silva, M. G. da & Camoes, A. R. 1981. Estudo faciológico dos afloramentos de Bom Despacho (BA): ritmitos e sedimentos de águas profundas associadas. *Rev. Bras. Geociênc.* **11**, 58–67.